Rock and Soil Mechanics

Volume 42 | Issue 2 Article 1

6-18-2021

One package of schemes for some difficult issues in finite element plasticity analysis

Hong ZHENG

Tan ZHANG

Qiu-sheng WANG

Custom Citation

ZHENG Hong, ZHANG Tan, WANG Qiu-sheng. One package of schemes for some difficult issues in finite element plasticity analysis[J]. Rock and Soil Mechanics, 2021, 42(2): 301-314.

Rock and Soil Mechanics 2021 42(2): 301−314 ISSN 1000−7598
https: //doi.org/10.16285/j.rsm.2020.6393 rocksoilmech.researchcommons.org/journal

One package of schemes for some difficult issues in finite element plasticity analysis

ZHENG Hong, ZHANG Tan, WANG Qiu-sheng

Key Laboratory of Urban Security and Disaster Engineering (Beijing University of Technology), Ministry of Education, Beijing 100124, China

Abstract: The Mohr-Coulomb yield criterion takes on the simplest form in the Mohr stress space, which has thus been most extensively applied in limit analysis and limit equilibrium methods because of its accuracy. However, the Mohr-Coulomb yield surface in the stress space is non-smooth, causing huge troubles to the constitutive integration in the deformation based finite element plasticity analysis. In addressing strength problems, meanwhile, solvers based on the load controlled method (LCM) are hard to bring the finite element model to the limit equilibrium state. Aiming at these issues, the solution schemes are proposed as follows. First, an algorithm named GSPC is designed for the constitutive integration for plasticity with non-smooth yield surfaces. GSPC is always convergent for arbitrary large strain increments, with far more excellent numerical properties than the return-mapping methods available. A solver based on the displacement controlled method (DCM) is developed fitted for the finite element plasticity analysis. The DCM solver is able to bring easily the finite element model into the limit equilibrium state, with no convergence issue, and far more efficient and robust than any LCM solvers. At the same time, a formula is derived for the computation of partial derivatives of principal stresses with respect to stress components. At last, combined with the strength reduction method, the secant method for the factor of safety of slopes is developed, and the location and depth of tension cracks at the slope top are proposed.

Keywords: constitutive integration for plasticity; Mohr-Coulomb yield surface; displacement controlled method; slope stability; tension cracks

1 Introduction

Strength problems include the evaluation of bearing capacity of ground foundations, the computation of lateral earth pressure on retaining walls, and the analysis of stability of slopes.

Classical methods for strength problems, such as the limit analysis and limit equilibrium methods, do not in general involve the computation of deformation. The Mohr-Coulomb yield criterion takes on its simplest form in the Mohr stress space. Meanwhile, the Mohr-Coulomb yield criterion has been in the dominant position of failure criteria of geomaterials because it is also very accurate.

However, the Mohr-Coulomb yield surface in the stress space is composed of six smooth surface patches. Those points on a ridge between two contiguous surface patches are non-smooth, in other words, normal lines at these points are not unique, which leads to huge troubles to the constitutive integration for plasticity in the deformation based finite element analysis. No tension cutting-off will increase the number of yield surface patches from six to nine, bringing in more troubles to the constitutive integration for plasticity. A quite large number of algorithms have been developed to address this issue, yet none of them is proved theoretically convergent. In practice, strain increments have to be made small enough to assure convergence and accuracy. Section 2 will deal with this issue.

The expression of yield surfaces in terms of principal stresses is usually simpler and easier visualized than the stress invariants and the Lode angle. In order to find out partial derivatives of yield functions or plastic potential functions with respect to stress components, however, partial derivatives of principal stresses with respect to stress components have to be computed. In the literature on solid mechanics, we have found no formulae available. We derive the relevant formulae in section 3, which are certainly of vital importance in the constitutive integration.

While the deformation based finite element analysis is applied to strength problems, usually geomaterials are deemed elastic perfectly plastic. Then, ground foundations or slopes are brought into the limit equilibrium state by increasing external loads or reducing material strength. At this moment, ground foundations or slopes in the limit equilibrium state turn actually into a mechanism; in other words, parts of ground foundations or slopes would slide along critical slip surfaces. In order to enhance robustness, even those very mature commercial software products decline the elastic perfectly plastic model. For example, Abaqus assigns a very small hardening modulus to the materials specified by the user to be elastic perfectly plastic. The Newton method for the system of nonlinear equilibrium equations is implemented by gradually increasing external loads, which is so called the load controlled method (LCM). Before ground foundations or slopes enter the limit equilibrium state, LCM is interrupted due to divergence. In section 4, an algorithm based on the displacement controlled method (DCM) is developed to aim at this issue. Combined with the strength reduction method, in section 5, the secant method for the factor of safety of slopes is developed, and the location and depth of tension cracks at the slope top are proposed. Section 6 illustrates

Received: 16 September 2020 Revised: 4 January 2021
This work was supported by the National Natural Science Foundation of China (52079002).
First author: ZHENG Hong, male, born in 1964, PhD, Professor, mainly engaged in teaching and research in numerical analysis of rock and soil mechanics. E-mail: hzheng@whrsm.ac.cn

applications of the proposed procedures to the stability analysis of slopes, pointing out the drawback of Michalowski's evaluation of depth of tension cracks at the top of slopes. Section 7 concludes with the prospects for the coming investigations.

2 Constitutive integration for plasticity with non-smooth yield surfaces

Figure 1(a) demonstrates the Mohr-Coulomb yield surface in the principal stress space of τ_1 - τ_2 - τ_3, which is composed of six planes. The intersection of the Mohr-Coulomb yield surface with the π-plane

$$\tau_1 + \tau_2 + \tau_3 = \text{constance}$$

is an irregular hexagon. Those points on a ridge between two contiguous planes are not smooth, i.e., normal lines at these points are not unique. As a result, there are huge difficulties in the constitutive integration for plasticity to either implicit algorithms[1] or explicit algorithms[2]. According to the associated flow rule, the plastic strain rate direction at a point on the yield surface is the outward normal line at the point. No tension cutting-off would result in the yield surface encompassed by nine yield surface patches, as shown in Fig. 1(b), which would further burden the constitutive integration.

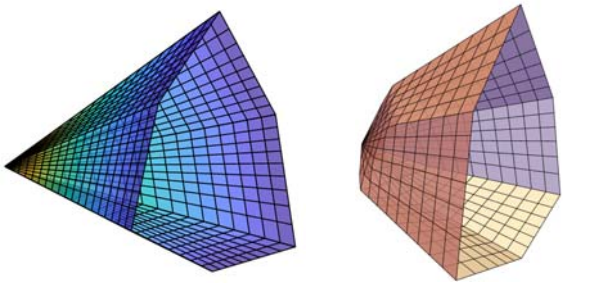

(a) M-C yielding surface (b) Cut-off M-C yielding surface

Fig. 1 Mohr-Coulomb yielding surfaces

Procedures for the constitutive integration with non-smooth yield surfaces can be roughly classified two categories. The first category is to smooth the non-smooth yield surface, and the second is to directly work with the non-smooth surface.

The Drucker-Prager yield surface is the simplest but coarsest smoothing approximation to the Mohr-Coulomb yield surface. By saying it is the simplest approximation to the Mohr-Coulomb yield surface, we mean the Drucker-Prager yield surface has the simplest and smoothest function expression. The intersection of the yield surface with the π plane is a circle. By saying it is the coarsest approximation to the Mohr-Coulomb yield surface, we mean the geomaterial followed by the Drucker-Prager yield criterion would have an equal tension strength and compression strength. The approximation of the Mohr-Coulomb yield surface by the Drucker-Prager yield surface is not unique. For example, we can specify the Drucker yield surface coincide with the major ridge or the minor ridge of the Mohr-Coulomb yield surface. It is more feasible to let the Drucker-Prager circle and the Mohr-Coulomb hexagon have an equal area[3]. The Drucker-Prager yield surface results, as it were, from global approximation to the Mohr-Coulomb yield surface.

In order to avert coarse errors created by the Drucker-Prager yield surface, since Zienkiewicz & Pande[4] and Menetrey & Willam[5], smoothing the Mohr-Coulomb yield surface has never halted[6–7], and the operations are locally smoothing. It is required that the smoothed yield surface be approximate sufficiently to the Mohr-Coulomb yield surface, convex and second order smooth. These requirements conflict to each other, as a result, it is not a trifle to have a satisfactory and locally smoothed Mohr-Coulomb yield surface. Smoothing incurs errors without exception, and compromises efficiency because the strain increment has to be small enough to assure convergence whenever the stress point is on the part of the yield surface with larger curvature.

The second category to cope with a non-smooth yield surface is to work directly with it. The simplest procedure is proposed by Owen et al.[8], in which the normal line at a point on a ridge of the Mohr-Coulomb yield surface is specified as the average of the two normal lines of the relevant surface patches. Such a practice only fits the explicit scheme because the divergence issue comes due to a discontinuous change of the normal line in the implicit scheme.

The return-mapping algorithms can be reduced to the solution of a system of non-smooth equations. The active yield surface patches are determined in iteration by a test-and-error process, and their convergence cannot be theoretically guaranteed. In practice, strain increments have to be small enough to reach convergence.

Reviews of the literature on constitutive integration for plasticity with non-smooth yield surfaces can be referred to[9] and monographs such as[10] and [11].

In this section, we reduce the constitutive integration for plasticity to a nonlinear complementarity problem and design the algorithm of GSPC. The convergence of GSPC can be theoretically guaranteed.

2.1 Perfectly elastic plastic constitutive relationship in the rate form

For an elastic plastic material, the stress rate vector $\dot{\boldsymbol{\sigma}}$ and the strain rate vector $\dot{\boldsymbol{\varepsilon}}$ are related by

$$\dot{\boldsymbol{\sigma}} = \boldsymbol{D}\left(\dot{\boldsymbol{\varepsilon}} - \dot{\boldsymbol{\varepsilon}}_{\mathrm{p}}\right) \tag{1}$$

Here, $\boldsymbol{D}$ is the symmetric and positive definite elastic matrix of 6×6; $\dot{\boldsymbol{\sigma}}$ and $\dot{\boldsymbol{\varepsilon}}$ are both 6-dimensional vectors; $\dot{\boldsymbol{\varepsilon}}$ are known with six components of $\dot{\varepsilon}_x$, $\dot{\varepsilon}_y$, $\dot{\varepsilon}_z$, $\dot{\gamma}_{yz}$, $\dot{\gamma}_{zx}$ and $\dot{\gamma}_{xy}$; $\dot{\boldsymbol{\sigma}}$ are unknown with the same subscripts as $\dot{\boldsymbol{\varepsilon}}$, with tension being specified positive. The plastic strain rate vector $\dot{\boldsymbol{\varepsilon}}_{\mathrm{p}}$ is unknown with the same subscripts as $\dot{\boldsymbol{\varepsilon}}$, determined by the Koiter flow rule[12]

$$\dot{\boldsymbol{\varepsilon}}_{\mathrm{p}} = \sum_{i=1}^{m} \lambda_i \nabla g_i \tag{2}$$

where m is the number of the yield surface patches

composing the yield surface; $\lambda_1, \cdots, \lambda_m$ are referred to as plastic multipliers that are not negative; $\nabla g_1, \cdots, \nabla g_m$ are gradients of the plastic potentials of $g_1, \cdots, g_m$ respectively, which are to be explained subsequently.

Except $\dot{\boldsymbol{\varepsilon}}$ and $\boldsymbol{D}$, all the quantities in Eqs. (1) and (2) depend nonlinearly on the current stress vector $\boldsymbol{\sigma}$ and the plastic multiplier vector $\boldsymbol{\lambda}$, written as $\dot{\boldsymbol{\sigma}}(\boldsymbol{\sigma},\boldsymbol{\lambda})$, $\dot{\boldsymbol{\varepsilon}}_{\mathrm{p}}(\boldsymbol{\sigma},\boldsymbol{\lambda})$ and $g_i(\boldsymbol{\sigma},\boldsymbol{\lambda})$. In order to sim-plify the equation expression, the arguments $(\boldsymbol{\sigma},\boldsymbol{\lambda})$ of $\dot{\boldsymbol{\sigma}}$ and others are totally omitted.

As for Eq.(2), more explanations are made as follows:

1) m is the number of the yield surface patches encompassing the elastic domain E_σ in the 6-dimensional stress space

$$E_\sigma \triangleq \left\{\boldsymbol{\tau} \in R^6 \,\middle|\, \boldsymbol{y}(\boldsymbol{\tau}) \leqslant 0\right\} \tag{3}$$

The symbol of "$\triangleq$" represents "is defined as"; $\boldsymbol{y}: R^6 \to R^m$ is a vector valued function that takes 6-dimensional vector of $\boldsymbol{\tau}$ as it argument and has m smooth component functions of $y_1(\boldsymbol{\tau})$, $\cdots$, $y_m(\boldsymbol{\tau})$, where $y_i(\boldsymbol{\tau}) = 0$ is the equation of the i-th boundary surface patch of E_σ; the yield function $y_i(\boldsymbol{\tau})$ is convex. In Eq.(3), $\boldsymbol{y}(\boldsymbol{\tau}) \leqslant 0$ means all the m component functions $y_i(\boldsymbol{\tau}) \leqslant 0$, $i = 1, \cdots, m$, suggesting that a stress point of $\boldsymbol{\tau}$ is only inside E_σ or on the surface of E_σ. Since merely elastic perfectly plastic materials are considered in this study, E_σ keeps invariant in the stress space.

Take the intact Mohr-Coulomb criterion as an instance. In the principal stress space of τ_1 - τ_2 - τ_3, E_σ is an irregular hexagon cone encompassed by six planes, as shown in Fig. 1(a). The six yield function are as follows:

$$\left.\begin{aligned}
y_1(\tau_1,\tau_2,\tau_3) &= (\tau_1 - \tau_3) + (\tau_1 + \tau_3)\sin\varphi - 2c\cos\varphi \\
y_2(\tau_1,\tau_2,\tau_3) &= (\tau_2 - \tau_3) + (\tau_2 + \tau_3)\sin\varphi - 2c\cos\varphi \\
y_3(\tau_1,\tau_2,\tau_3) &= (\tau_2 - \tau_1) + (\tau_2 + \tau_1)\sin\varphi - 2c\cos\varphi \\
y_4(\tau_1,\tau_2,\tau_3) &= (\tau_3 - \tau_1) + (\tau_3 + \tau_1)\sin\varphi - 2c\cos\varphi \\
y_5(\tau_1,\tau_2,\tau_3) &= (\tau_3 - \tau_2) + (\tau_3 + \tau_2)\sin\varphi - 2c\cos\varphi \\
y_6(\tau_1,\tau_2,\tau_3) &= (\tau_1 - \tau_2) + (\tau_1 + \tau_2)\sin\varphi - 2c\cos\varphi
\end{aligned}\right\} \tag{4}$$

in which c is the cohesion and φ the internal frictional angle. E_σ encompassed by the Mohr-Coulomb yield surface has six ridges and one vertex, points on which are not smooth. Particularly, by taking $\varphi = 0$, the Mohr-Coulomb yield criterion reduces to the Tresca yield criterion, which fits the transient case with no drainage.

If the material cannot bear tension, what we obtain is the cut-off Mohr-Coulomb yield surface, as shown in Fig. 1(b). E_σ in the principal stress space has another three planes:

$$\left.\begin{aligned}
y_7(\tau_1,\tau_2,\tau_3) &= \tau_1 \\
y_8(\tau_1,\tau_2,\tau_3) &= \tau_2 \\
y_9(\tau_1,\tau_2,\tau_3) &= \tau_3
\end{aligned}\right\} \tag{5}$$

In this case, the number of the surface patches composing the cut-off Mohr-Coulomb yield surface is nine, i.e., m=9, and more ridges and vertices are created.

2) Correspondent to the i-th yield surface patch $y_i(\boldsymbol{\tau}) = 0$ is the i-th plastic potential function $g_i(\boldsymbol{\tau})$. The Koiter flow rule defined by Eq. (2) says that $\dot{\boldsymbol{\varepsilon}}_{\mathrm{p}}$ can be expressed by the non-negative linear composition of gradients of all the m potential functions, $\nabla g_i(\boldsymbol{\sigma})$, $i = 1, \cdots, m$. More explanations will be given shortly.

3) If taking $g_i = y_i$, the flow rule defined by Eq. (2) is called the associated flow rule; otherwise, the non-associative flow rule. By taking the Mohr-Coulomb material as an instance, and replacing the internal frictional angle φ by the dilatancy angle ψ, the potential function $g_i(\boldsymbol{\tau})$ is obtained, with $0 \leqslant \psi \leqslant \varphi$.

4) The stress point $\boldsymbol{\sigma}$ evolves according to Eq. (1). Meanwhile, at no time is $\boldsymbol{\sigma}$ outside E_σ; or in other words, $\boldsymbol{y}(\boldsymbol{\sigma}) \leqslant 0$.

In Eq. (2), λ_i and $-y_i$ constitute a pair of relationship, namely,

$$\lambda_i \geqslant 0,\ -y_i \geqslant 0,\ \lambda_i(-y_i) = 0 \tag{6}$$

for $i = 1, \cdots, m$; or the vector form equivalent to Eq. (6)

$$0 \leqslant \boldsymbol{\lambda} \perp (-\boldsymbol{y}) \geqslant 0 \tag{7}$$

where $\boldsymbol{\lambda}$ is an m-dimensional vector with m components of $\lambda_1, \cdots, \lambda_m$. Here, "$\perp$" represents "perpendicular to"; that is to say, "$\boldsymbol{a} \perp \boldsymbol{b}$" is equivalent to "$\boldsymbol{a}^{\mathrm{T}}\boldsymbol{b} = 0$".

Particularly, if $\boldsymbol{y}(\boldsymbol{\sigma}) < 0$, namely, the stress point $\boldsymbol{\sigma}$ is inside E_σ, then $\boldsymbol{\lambda} = 0$ according to the complementarity relationship (7), and $\dot{\boldsymbol{\varepsilon}}_{\mathrm{p}} = 0$ is implied according to Eq.(2), suggesting $\dot{\boldsymbol{\sigma}}$ is dependent linearly upon $\dot{\boldsymbol{\varepsilon}}$.

Otherwise, if the stress point $\boldsymbol{\sigma}$ is on the boundary of E_σ, then two cases exist:

1) $\boldsymbol{\sigma}$ is on only one yield surface patch, e.g., the first yield function surface of $y_1(\boldsymbol{\sigma}) = 0$, while $y_i(\boldsymbol{\sigma}) < 0$, $i = 2, \cdots, m$; namely, the yield surface at $\boldsymbol{\sigma}$ is smooth. According to the complementarity relation (6), $\lambda_1 \geqslant 0$, while $\lambda_i = 0$, $i = 2, \cdots, m$. By the Koiter rule (2), the strain rate vector $\dot{\boldsymbol{\varepsilon}}_{\mathrm{p}}$ is in direction of $\nabla g_1(\sigma)$.

2) $\boldsymbol{\sigma}$ is on the ridge of the first and second patch, say, implying $y_1(\boldsymbol{\sigma}) = y_2(\boldsymbol{\sigma}) = 0$; while $y_i(\boldsymbol{\sigma}) < 0$, $i = 3, \cdots, m$. According to the complementarity relation (6), $\lambda_1 \geqslant 0$ and $\lambda_2 \geqslant 0$, while $\lambda_i = 0$, $i = 3, \cdots, m$. By the Koiter rule (2), $\dot{\boldsymbol{\varepsilon}}_{\mathrm{p}}$ must be located in the normal cone $V(\boldsymbol{\sigma})$ at $\boldsymbol{\sigma}$ corresponding to the two plastic potential contours

$g_1(\boldsymbol{\sigma})=\text{constant\_1}$ and $g_2(\boldsymbol{\sigma})=\text{constant\_2}$

Here, if $\boldsymbol{\xi}\in V(\boldsymbol{\sigma})$, then there exist two non-negatives α and β, such that

$$\boldsymbol{\xi}=\alpha\nabla g_1(\boldsymbol{\sigma})+\beta\nabla g_2(\boldsymbol{\sigma})$$

Especially for the associated flow rule, the Koiter rule defined by Eqs. (2) and (7) states that the strain rate vector $\dot{\boldsymbol{\varepsilon}}_{\mathrm{p}}$ always belongs to the normal cone $V(\boldsymbol{\sigma})$ of E_σ at point $\boldsymbol{\sigma}$, which is defined as follows. If $\boldsymbol{\sigma}$ is inside E_σ, $V(\boldsymbol{\sigma})=\{0\}$. If $\boldsymbol{\sigma}$ is only on the first yield patch $y_1(\boldsymbol{\sigma})=0$, say, all the vectors in $V(\boldsymbol{\sigma})$ are in direction of vector $\nabla y_1(\boldsymbol{\sigma})$. If $\boldsymbol{\sigma}$ is on the ridge between the two patches of $y_2(\boldsymbol{\sigma})=0$ and $y_3(\boldsymbol{\sigma})=0$, say, then all the vectors in $V(\boldsymbol{\sigma})$ are the non-negative linear combination of the two vectors $\nabla y_2(\boldsymbol{\sigma})$ and $\nabla y_3(\boldsymbol{\sigma})$. Figure 2 shows the normal cones of the stress points at three different positions: $\boldsymbol{\sigma}_1$ is inside E_σ; $\boldsymbol{\sigma}_2$ is only on the yield surface patch $y_1(\boldsymbol{\sigma})=0$ of E_σ; and $\boldsymbol{\sigma}_3$ is on the ridge of the two boundary patches $y_2(\boldsymbol{\sigma})=0$ and $y_3(\boldsymbol{\sigma})=0$ of E_σ.

The substitution of Eq. (2) into Eq. (1) leads to

$$\dot{\boldsymbol{\sigma}}=\dot{\boldsymbol{\sigma}}_{\mathrm{e}}-\boldsymbol{\sigma}_{\mathrm{p}} \tag{8}$$

with

$$\dot{\boldsymbol{\sigma}}_{\mathrm{e}}\triangleq\boldsymbol{D}\dot{\boldsymbol{\varepsilon}} \tag{9}$$

and

$$\boldsymbol{\sigma}_{\mathrm{p}}\triangleq\boldsymbol{D}\boldsymbol{J}\boldsymbol{\lambda} \tag{10}$$

Here, $\boldsymbol{J}$ is Jacobean of the vector valued function $\boldsymbol{g}$: $R^6\to R^m$, a matrix of 6×m; and $\boldsymbol{g}$ has m component functions which are the m plastic potential functions of g_1, ⋯, g_m; so,

$$\boldsymbol{J}(\boldsymbol{\sigma})\triangleq\left[\nabla g_1(\boldsymbol{\sigma}),\cdots,\nabla g_m(\boldsymbol{\sigma})\right] \tag{11}$$

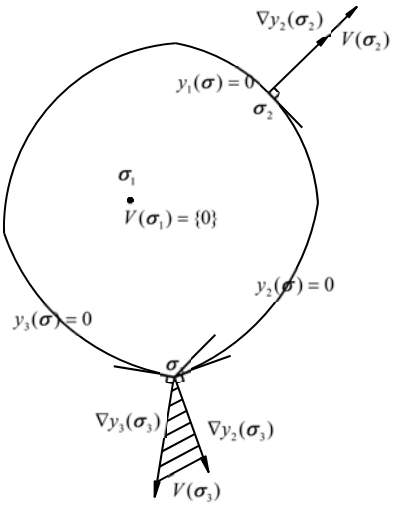

Fig. 2 Schematic of normal cones at different points

To this point, Eqs. (8) and (7) (or Eq. (6)) describe elastic and perfectly plastic deformation in the rate form, which constitute the differential-algebraic equations, DAE for short. However, the algebraic equations here are in the complementarity form; as a result, we propose calling them the differential-complementary equations, with the acronym of DCE. According to our searching, no such a term exists in the literature. Because the algebraic equations in the conventional DAE are usually smooth, the general solutions for DAE, such as literature[13], are not able to be directly applied to the DCE just introduced.

The numbers of the differential Eqs. (8) and the complementarity Eqs. (7) are 6 and m, just equaling the number of components of vectors $\boldsymbol{\sigma}$ and $\boldsymbol{\lambda}$, i.e., the 6 components of the stress vector $\boldsymbol{\sigma}$ and the m plastic multipliers of vector $\boldsymbol{\lambda}$. So, once the initial value $\boldsymbol{\sigma}_0$ of $\boldsymbol{\sigma}$ is given, in principle $\boldsymbol{\sigma}$ and $\boldsymbol{\lambda}$ corresponding to the finite strain increment of $\Delta\boldsymbol{\varepsilon}$ can be derived.

2.2 The numerical constitutive integration

Now suppose the time interval corresponding to the current load increment is $(0,T]$. We will shortly see T can be any real greater than zero, i.e., the so-called pseudo time length. The strain rate $\dot{\boldsymbol{\varepsilon}}$ and T are related by

$$\dot{\boldsymbol{\varepsilon}}=\frac{\Delta\boldsymbol{\varepsilon}}{T} \tag{12}$$

The formulation of the constitutive integration is stated as follows. Suppose the initial value $\boldsymbol{\sigma}_0$ of $\boldsymbol{\sigma}$ and the strain increment $\Delta\boldsymbol{\varepsilon}$ of this load step are given, find out the total stress vector $\boldsymbol{\sigma}_{\mathrm{T}}$. In order to limit the introduction of too many notations, $\boldsymbol{\sigma}_{\mathrm{T}}$ is still written as $\boldsymbol{\sigma}$.

Integration of Eq. (8) with respect to time over the interval of $(0,T]$ by using the Euler backward integration leads to

$$\boldsymbol{\sigma}=\boldsymbol{\sigma}_{\mathrm{e}}-T\boldsymbol{\sigma}_{\mathrm{p}} \tag{13}$$

in which $\boldsymbol{\sigma}_{\mathrm{e}}$ is the elastic trial stress

$$\boldsymbol{\sigma}_{\mathrm{e}}\triangleq\boldsymbol{\sigma}_0+\boldsymbol{D}\Delta\boldsymbol{\varepsilon} \tag{14}$$

where both $\boldsymbol{J}$ and $\boldsymbol{\lambda}$ in $\boldsymbol{\sigma}_{\mathrm{p}}$, see Eq. (10), are calculated at time T.

Considering $T\boldsymbol{\sigma}_{\mathrm{p}}=\boldsymbol{D}\boldsymbol{J}(T\boldsymbol{\lambda})$, and Eq. (7) still holds by replacing $\boldsymbol{\lambda}$ with $T\boldsymbol{\lambda}$, i.e.,

$$0\leqslant T\boldsymbol{\lambda}\perp(-\boldsymbol{y})\geqslant 0 \tag{15}$$

As a result, what we can find out from Eqs. (13) and (15) are $T\boldsymbol{\lambda}$ but not $\boldsymbol{\lambda}$. This, however, does not affect the value of $\boldsymbol{\sigma}$.

The above deduction just reflects the following feature of rate-independent materials (or quasi-static problems): the increment stress vector $\Delta\boldsymbol{\sigma}$ is independent of the magnitude of time length T, but dependent on the increment strain vector $\Delta\boldsymbol{\varepsilon}$. According to the authors' knowledge from the literature,

it is the first time to prove $\Delta\boldsymbol{\sigma}$ is independent of time step length T by explicitly introducing time variable t and its interval $(0,T]$ and integrating rate constitutive Eqs. (1) of plasticity.

Therefore, in order to pursue compact formulation, we deem $T\boldsymbol{\lambda}$ as $\boldsymbol{\lambda}$, and rewrite Eq. (13) into

$$\boldsymbol{\sigma}=\boldsymbol{\sigma}_{\mathrm{e}}-\boldsymbol{\sigma}_{\mathrm{p}} \tag{16}$$

with $\boldsymbol{\sigma}_{\mathrm{p}}$ being defined by Eq.(10). Afterwards, Eq. (16) is termed as the decomposition of elastic-plastic stress, which is of vital importance in deriving the alternative form of the finite element system of nonlinear equations in section 4.

To this point, we have obtained the system (16) of nonlinear equations and nonlinear complementarity relationship (7) for determining $(\boldsymbol{\sigma},\boldsymbol{\lambda})$, which will constitute the mixed complementarity problem to be introduced in the next subsection.

2.3 The mixed complementarity problem and the solution algorithm of GSPC

To sum up, the mixed complementarity problem arising from the constitutive integration for plasticity can be stated as follows. Given the strain increment vector $\Delta\boldsymbol{\varepsilon}$, find $(\boldsymbol{\sigma},\boldsymbol{\lambda})\in R^6\times R_+^m$ such that

$$\left.\begin{aligned}&0\leqslant\boldsymbol{\lambda}\perp\boldsymbol{f}_I(\boldsymbol{\sigma},\boldsymbol{\lambda})\geqslant 0\\&\boldsymbol{f}_E(\boldsymbol{\sigma},\boldsymbol{\lambda})=0\end{aligned}\right\} \tag{17}$$

which is abbreviated by MiCP $(\boldsymbol{f}_I,\boldsymbol{f}_E)$. Here, R_+^m represents the nonnegative orthant of R^n; in other words, all the m components of any vector in R_+^m are nonnegative. $\boldsymbol{f}_I: R^6\times R_+^m\to R^m$ is defined by

$$\boldsymbol{f}_I(\boldsymbol{\sigma},\boldsymbol{\lambda})\triangleq-\boldsymbol{y}(\boldsymbol{\sigma}) \tag{18}$$

$\boldsymbol{f}_E: R^6\times R_+^m\to R^6$ by

$$\boldsymbol{f}_E(\boldsymbol{\sigma},\boldsymbol{\lambda})\triangleq\boldsymbol{\sigma}+\boldsymbol{\sigma}_{\mathrm{p}}-\boldsymbol{\sigma}_{\mathrm{e}} \tag{19}$$

Supposing the set of solutions to MiCP $(\boldsymbol{f}_I,\boldsymbol{f}_E)$ is not empty, the following results have been obtained in Ref[14]:

1) for the associated flow, the solution to MiCP $(\boldsymbol{f}_I,\boldsymbol{f}_E)$ is unique;

2) for the non-associated flow, a sufficient condition to guarantee the uniqueness of solution to MiCP $(\boldsymbol{f}_I,\boldsymbol{f}_E)$ is given; and

3) even for the non-associated flow, the solution to MiCP $(\boldsymbol{f}_I,\boldsymbol{f}_E)$ is still unique if the cut-off Mohr-Coulomb yield surface is applied.

Applying the fact that MiCP $(\boldsymbol{f}_I,\boldsymbol{f}_E)$ is a particular case of finite dimensional variational inequalities and using the Gauss-Seidel iteration skill, we improved the projection-contraction algorithm for general finite dimensional variational inequalities[15], and called the improved algorithm GSPC that owns the following features:

1) GSPC is always convergent for an arbitrary large strain increment $\Delta\boldsymbol{\varepsilon}$; while the return-mapping algorithm is not always convergent even if $\Delta\boldsymbol{\varepsilon}$ is small enough.

2) GSPC does not need to test if the elastic trial stress $\boldsymbol{\sigma}_{\mathrm{e}}$ is outside the elastic domain E_σ; nor to find the intersection of the elastic path $\boldsymbol{\sigma}_0$-$\boldsymbol{\sigma}_{\mathrm{e}}$ with the yield surface; nor to guess which yield surface patches are active; and nor to compute the Hesse of the plastic potential function g_i.

And 3) GSPC is more efficient than the return-mapping algorithm; what is more, such an advantage becomes more obvious for non-smooth yield surfaces.

Since no trial-and-error process is involved, programming GSPC is even simpler than the Gauss elimination method. For the sake of integrity, the pseudocodes of GSPC are listed in the appendix.

If a return-mapping algorithm is applied to solve $(\boldsymbol{\sigma},\boldsymbol{\lambda})$ and if $\boldsymbol{\sigma}_{\mathrm{e}}$ is outside E_σ, usually the intersection $\boldsymbol{\sigma}_I$ of the elastic path $\boldsymbol{\sigma}_0$-$\boldsymbol{\sigma}_{\mathrm{e}}$ with the yield surface is needed(see Fig.3), which needs to take some computations.

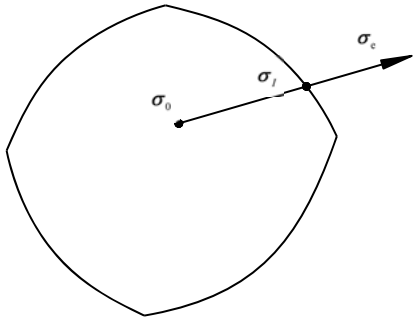

Fig. 3 Intersection $\boldsymbol{\sigma}_I$ of elastic path $\boldsymbol{\sigma}_0$-$\boldsymbol{\sigma}_{\mathrm{e}}$ and the yielding surface

Even if the yield surface is smooth, such as the Mises yield surface, in order for the return-mapping algorithm to be convergent and accurate, the strain increment vector $\Delta\boldsymbol{\varepsilon}$ has to be small enough.

If the return-mapping algorithm is applied to address non-smooth yield surfaces, the assumption of the active yield surfaces is needed. If the 4th and 5th yield surface patches are assumed active, then the return-mapping algorithm needs to solve the system of nonlinear equations in $\boldsymbol{\sigma}$, λ_4 and λ_5

$$\left.\begin{aligned}&\boldsymbol{\sigma}=\boldsymbol{\sigma}_{\mathrm{e}}-\boldsymbol{D}\left[\lambda_4\nabla g_4(\boldsymbol{\sigma})+\lambda_5\nabla g_5(\boldsymbol{\sigma})\right]\\&f_4(\boldsymbol{\sigma})=0\\&f_5(\boldsymbol{\sigma})=0\end{aligned}\right\} \tag{20}$$

which is equivalent to the mixed complementarity problem (17) because $\lambda_i=0$ for any $i\neq 4$ or 5.

If both λ_4 and λ_5 are nonnegative, then the assumption that the 4th and 5th yield surface patches are active is right; otherwise, other yield surface patches are specified active and the new iteration process is started[11].

If the Newton method is used to solve system (20), the Hesse matrices of g_4 and g_5

$$\left(\frac{\partial^2 g_4}{\partial\tau_i\partial\tau_j}\right)_{\boldsymbol{\tau}=\boldsymbol{\sigma}} \text{ and} \left(\frac{\partial^2 g_5}{\partial\tau_i\partial\tau_j}\right)_{\boldsymbol{\tau}=\boldsymbol{\sigma}} \tag{21}$$

have to be calculated. Here, the subscripts of *i* and *j* range from 1 to 6, referring to anyone of the six components: τ_x , τ_y , τ_z , τ_{yz} , τ_{zx} , τ_{xy} ; for example,

$$\frac{\partial^2 g_4}{\partial\tau_2\partial\tau_4}=\frac{\partial^2 g_4}{\partial\tau_y\partial\tau_{yz}}$$

and so on.

Obviously, the more the patches encompassing E_σ are, the more complicated the return-mapping algorithm will become. Take the cut-off Mohr-Coulomb yield surface for an instance. At most three active yield surface patches might be active. What is worse, the return-mapping algorithm is not able to assure convergence. Luckily, GSPC has totally solved these issues.

3 Partial derivatives of principal stresses with respect to stress components

For many yield surfaces, the expressions of the yield functions and plastic potential functions are far simpler and more intuitive in the 3-dimensional principal stress space than in the 6-dimensional stress space in terms of the stress invariants and the Lode angle. According to the Koiter flow rule(Eq.(2)) and the chain rule of derivation, the computation of the partial derivative of the plastic potential function *g* with respect to the stress component σ_{ij} necessitates the computation of the partial derivatives of the three principal stresses with respect to σ_{ij} , namely,

$$\frac{\partial g}{\partial\sigma_{ij}}=\sum_{k=1}^{3}\frac{\partial g}{\partial\sigma_k}\frac{\partial\sigma_k}{\partial\sigma_{ij}} \tag{22}$$

where, σ_k , $k = 1, 2, 3$, are the three principal stresses. In the literature on solid mechanics, we have found no formula or algorithm for computing $\frac{\partial\sigma_k}{\partial\sigma_{ij}}$. Now we will fill the gap.

Let the 3×3 matrix of the stress tensor be denoted by $\boldsymbol{S}$, i.e.,

$$\boldsymbol{S}=\begin{bmatrix}\sigma_x & \tau_{xy} & \tau_{xz}\\ \tau_{yx} & \sigma_y & \tau_{yz}\\ \tau_{zx} & \tau_{zy} & \sigma_z\end{bmatrix} \tag{23}$$

Since $\tau_{xy}=\tau_{yx}$, etc., $\boldsymbol{S}$ is symmetric.

Further, denote by σ anyone of the three principal stresses, and by $\boldsymbol{l}$ the relevant principal direction of σ . Then,

$$\boldsymbol{S}\boldsymbol{l}=\sigma\boldsymbol{l} \tag{24}$$

By differentiating the both sides of the above equation with respect to any stress component, we have

$$\boldsymbol{S}'\boldsymbol{l}+\boldsymbol{S}\boldsymbol{l}'=\sigma'\boldsymbol{l}+\sigma\boldsymbol{l}' \tag{25}$$

Here, $\boldsymbol{S}'$ represents the partial derivative of $\boldsymbol{S}$ with respect to the stress component; for example, in the computation of the partial derivative of $\boldsymbol{S}$ with respect to σ_y , $\boldsymbol{S}'$ represents

$$\boldsymbol{S}'=\frac{\partial\boldsymbol{S}}{\partial\sigma_y}=\begin{bmatrix}0&0&0\\0&1&0\\0&0&0\end{bmatrix}$$

For another example, in the computation of the partial derivative of $\boldsymbol{S}$ with respect to τ_{xy} , $\boldsymbol{S}'$ represents

$$\boldsymbol{S}'=\frac{\partial\boldsymbol{S}}{\partial\tau_{xy}}=\begin{bmatrix}0&1&0\\1&0&0\\0&0&0\end{bmatrix}$$

and so on.

Pre-multiplication of the both sides of Eq. (25) by $\boldsymbol{l}^{\mathrm{T}}$ leads to

$$\boldsymbol{l}^{\mathrm{T}}\boldsymbol{S}'\boldsymbol{l}+\boldsymbol{l}^{\mathrm{T}}\boldsymbol{S}\boldsymbol{l}'=\sigma'\boldsymbol{l}^{\mathrm{T}}\boldsymbol{l}+\sigma\boldsymbol{l}^{\mathrm{T}}\boldsymbol{l}' \tag{26}$$

From $\boldsymbol{l}^{\mathrm{T}}\boldsymbol{l}=1$ and by differentiating both its sides, $\boldsymbol{l}^{\mathrm{T}}\boldsymbol{l}'=0$ is deduced. Meanwhile, $\boldsymbol{S}=\boldsymbol{S}^{\mathrm{T}}$ and Eq. (24) imply

$$\boldsymbol{l}^{\mathrm{T}}\boldsymbol{S}\boldsymbol{l}'=\left(\boldsymbol{S}\boldsymbol{l}\right)^{\mathrm{T}}\boldsymbol{l}'=\sigma\boldsymbol{l}^{\mathrm{T}}\boldsymbol{l}'=0 \tag{27}$$

Finally, Eq. (26) can be reduced to

$$\sigma'=\boldsymbol{l}^{\mathrm{T}}\boldsymbol{S}'\boldsymbol{l} \tag{28}$$

Specifically, we have

$$\left.\begin{aligned}&\frac{\partial\sigma}{\partial\sigma_x}=\boldsymbol{l}^{\mathrm{T}}\frac{\partial\boldsymbol{S}}{\partial\sigma_x}\boldsymbol{l}=l_x^2,\ \frac{\partial\sigma}{\partial\sigma_y}=l_y^2,\ \frac{\partial\sigma}{\partial\sigma_z}=l_z^2,\\ &\frac{\partial\sigma}{\partial\tau_{xy}}=\boldsymbol{l}^{\mathrm{T}}\frac{\partial\boldsymbol{S}}{\partial\tau_{xy}}\boldsymbol{l}=2l_xl_y,\ \frac{\partial\sigma}{\partial\tau_{yz}}=2l_yl_z,\ \frac{\partial\sigma}{\partial\tau_{zx}}=2l_zl_x\end{aligned}\right\} \tag{29}$$

with $\left(l_x,l_y,l_z\right)=\boldsymbol{l}^{\mathrm{T}}$. In short,

$$\frac{\partial\sigma_k}{\partial\sigma_{ij}}=\left(2-\delta_{ij}\right)l_i^kl_j^k \tag{30}$$

with $i,j,k=1,2,3$ and $\boldsymbol{l}^k$ = unit principal direction corresponding to the *k*th principal stress σ_k . δ_{ij} is the Kronecker-Delta. Note that no summation is implied over the repeated indices *i*, *j*, or *k*.

It must be noted that applying the transforms between components of the stress tensor in the framework composed of the three principal directions and the user defined coordinate system, Yang et al.[16] derived the same results as Eq. (29), which is not familiar to the authors until the submission of this manuscript. Since the derivation is quite different from literature [16], this section is still retained.

4 The displacement-controlled method

When a ground foundation or a slope composed of elastic perfectly plastic materials reaches the limit equilibrium state, the ground foundation or the slope will turn into a mechanism because the critical slip surface runs through the model; in other words, part of the ground foundation or the slope will slide along the critical slip surface. At this moment, the tangential stiffness matrix will be no longer positively definite and have a rank deficiency of one[17], rendering the Newton method based on the load-controlled method (LCM) to fail to converge. As a matter of fact, even prior to the limit equilibrium state, the LCM is usually hard to converge.

In order to bring the discretization model into the limit equilibrium state, we need to solve the system of equilibrium equations in FEA by the displacement-controlled method (DCM). But big differences in the programming structure exist between LCM and DCM. As a result, the DCM is seldom applied by programmers.

In this section, a solver will be designed especially for the finite element plasticity analysis. Based on the solver, the LCM and DCM can have structures very analogous to each other, and it is quite convenient to switch between LCM and DCM.

4.1 Alternative form of FEA system of equilibrium equations

Once the problem domain Ω is discretized in a set of finite elements, we are always able to set up the system of equilibrium equations

$$\sum_{\mathrm{e}} \int_{\Omega^{\mathrm{e}}} \boldsymbol{B}^{\mathrm{T}} \boldsymbol{\sigma} \mathrm{d}\Omega = \boldsymbol{q} + \boldsymbol{q}_0 \tag{31}$$

at the end of the current load step. Here, $\boldsymbol{q}_0$ represents the equivalent load vector at the beginning of the current load step; $\boldsymbol{q}$ the incremental equivalent load vector at the end of the current load step. That means $\boldsymbol{q}+\boldsymbol{q}_0$ represents the load level at the end of the current load step; Σ represents the summation in the sense of assemblage; Ω^{e} is a typical element in the mesh; $\boldsymbol{\sigma}$ is the total stress vector at the end of the current load step; and $\boldsymbol{B}$ is the $6\times n_{\mathrm{e}}$ matrix that transforms the incremental displacement degrees of freedom vector $\boldsymbol{p}_{\mathrm{e}}$ of element Ω^{e} into the incremental strain vector $\Delta\boldsymbol{\varepsilon}$, i.e.,

$$\Delta\boldsymbol{\varepsilon} = \boldsymbol{B}\boldsymbol{p}_{\mathrm{e}} \tag{32}$$

with n_{e} = dimension of vector $\boldsymbol{p}_{\mathrm{e}}$.

In the literature on FEM such as [12], the computations of $\boldsymbol{B}$, $\boldsymbol{q}$ and $\boldsymbol{q}_0$ are expounded upon.

However, the application of $\boldsymbol{q}+\boldsymbol{q}_0$ to the set of finite elements at a stroke might be hard to converge. In practice, we usually introduce a load multiplier ρ less than one, followed by solving the system of equilibrium equations

$$\sum_{\mathrm{e}} \int_{\Omega^{\mathrm{e}}} \boldsymbol{B}^{\mathrm{T}} \boldsymbol{\sigma} \mathrm{d}\Omega = \rho\boldsymbol{q} + \boldsymbol{q}_0 \tag{33}$$

which is corresponding to the load level of $\rho\boldsymbol{q}+\boldsymbol{q}_0$. After the convergence is reached, the displacement increments, the stresses and $\boldsymbol{q}_0$, and so on, are updated, i. e., $\boldsymbol{q}_0 := \rho\boldsymbol{q}+\boldsymbol{q}_0$. Then, the above process is repeated till $\sum\rho$ equals one. This is just the LCM. If $\sum\rho$ cannot reach the value of 1, the value of $\sum\rho$ is the limit load multiplier that the LCM is able to seek. In general, clearly, the LCM fails to converge even in advance of the limit state. As a result, $\sum\rho$ is always below the real limit load multiplier using LCM.

It is supposed the incremental displacement degrees of freedom vector is $\boldsymbol{p}$ due to the application of $\boldsymbol{q}$, with $\boldsymbol{p}\in R^n$. If $\boldsymbol{p}$ is taken as the primal variable, then the system (33) is the system of nonlinear equations in $\boldsymbol{p}$, where $\boldsymbol{\sigma}$ is nonlinearly dependent on $\boldsymbol{p}$. The LCM for system (33) is usually the Newton method, creating a quite diffenent programming structure from DCM. In order to be convenient to switch from LCM to DCM, we propse applying the more efficient method to solve system (33) as follows.

The substitution of the decomposition (16) of elastic-plastic stresses, together with Eqs. (14), (10) and (32) into Eq. (33) leads to the system of nonlinear equations in $\boldsymbol{p}$

$$\boldsymbol{K}\boldsymbol{p} = \rho\boldsymbol{q} + \boldsymbol{r} \tag{34}$$

where $\boldsymbol{K}$ is the elastic stiffness matrix

$$\boldsymbol{K} \triangleq \sum_{\mathrm{e}} \int_{\Omega^{\mathrm{e}}} \boldsymbol{B}^{\mathrm{T}} \boldsymbol{D} \boldsymbol{B} \mathrm{d}\Omega \tag{35}$$

$\boldsymbol{K}$ keeps invariant during the iteration of system (34); vector $\boldsymbol{r}$ depends nonlinearly upon $\boldsymbol{p}$, reading

$$\boldsymbol{r} \triangleq \overline{\boldsymbol{q}}_0 + \sum_{\mathrm{e}} \int_{\Omega^{\mathrm{e}}} \boldsymbol{B}^{\mathrm{T}} \boldsymbol{\sigma}_{\mathrm{p}} \mathrm{d}\Omega \tag{36}$$

with $\boldsymbol{\sigma}_{\mathrm{p}}$ defined by Eq.(10), but $\overline{\boldsymbol{q}}_0$ keeping invariant, defined by

$$\overline{\boldsymbol{q}}_0 \triangleq \boldsymbol{q}_0 - \sum_{\mathrm{e}} \int_{\Omega^{\mathrm{e}}} \boldsymbol{B}^{\mathrm{T}} \boldsymbol{\sigma}_0 \mathrm{d}\Omega \tag{37}$$

In LCM, ρ is given. The system (34) has an equal number of equations and unknowns, denoted by n. Each equation in system (34) represents a surface in R^n, with the n components of vector $\boldsymbol{p}$ acting as coordinates. The solution of system (34) is actually to find the intesection of the n surfaces. The coordinate vector of the intersection is just $\boldsymbol{p}$. If the set of finite elements is approaching the limit equilibrium state, the LCM will be incapable of convergence. At this moment, we need to turn to the DCM. Here is the idea of the DCM.

If ρ is deemed unknown, the system (34) includes n equations but $n+1$ unknowns, i.e., $(\boldsymbol{p},\rho)$, which define a curve C in R^{n+1}, called the equilibrium path. The curve C is the intersection of the n surfaces in system (34). The LCM is actually to cut the curve C with a series of super-planes of "ρ =constant". As a result, only if ρ can act as the parameter of curve C, or in other words, only if curve C is not parallel to the plane of "ρ =constant", it is possible to cut curve C

with a plane of "ρ =constant"; or equivalently, to trace curve *C* using LCM. Otherwise, no intersection exists because a plane of "ρ =constant" is parallel to curve *C*, causing the LCM to fail to converge.

In order to continue tracing curve *C*, we let a component of $\boldsymbol{p}$, say p_i, be given, while ρ unknown, to solve system (34). This is actually to cut curve *C* with a series of planes of "p_i =constant", which is just the DCM.

Instead of the Newton method, the direct iteration method is applied to system (34) under the condition that p_i is given. In iteration, vector $\boldsymbol{r}$ is regarded as a known quantity that depends on the former iterate $\boldsymbol{p}^k$ of $\boldsymbol{p}$, which leads to the iteration scheme of system (34)

$$\boldsymbol{K}\boldsymbol{p}^{k+1} = \rho^{k+1}\boldsymbol{q} + \boldsymbol{r}^k \tag{38}$$

with the superscripts of k and k+1 being the iteration number. In this way, the coefficient matrix $\boldsymbol{K}$ is always symmetric and positively definite for either the associated flow or the non-associated flow. As is well known, in the case of the non-associated flow, the tangential stiffness matrix is asymmetric. Consequently, the proposed solution is at least superior in memory storage to the conventional tangential stiffness matrix. Moreover, the condition number of the tangential stiffness matrix in LCM becomes bigger and bigger while approaching to the limit state, causing worse and worse the numerical property of the relevant system of linear equations in LCM. However, the iterative scheme (38) overcomes completely this problem, because the elastic matrix $\boldsymbol{K}$ is always best in the aspect of numerical properties amongst all the tangential stiffness matrices. As a result, the proposed DCM enjoys much better numerical properties than the LCM with tangential stiffness matrices.

Pre-multiplying both the sides of system (38) with $\boldsymbol{K}^{-1}$, we have

$$\boldsymbol{p}^{k+1} = \rho^{k+1}\boldsymbol{p}_q + \boldsymbol{p}_r^k \tag{39}$$

Here, $\boldsymbol{p}_q$ is the elastic displacement vector due to the load $\boldsymbol{q}$, namely, $\boldsymbol{p}_q$ is the solution to the system

$$\boldsymbol{K}\boldsymbol{p}_q = \boldsymbol{q} \tag{40}$$

and $\boldsymbol{p}_q$ also keeps invariant during iteration. $\boldsymbol{p}_r^k$ in system (41) is the elastic displacement vector due to the load $\boldsymbol{r}^k$, i.e., the solution to system

$$\boldsymbol{K}\boldsymbol{p}_r^k = \boldsymbol{r}^k \tag{41}$$

and $\boldsymbol{p}_r^k$ depends on $\boldsymbol{\sigma}_{\mathrm{p}}^k$, while $\boldsymbol{\sigma}_{\mathrm{p}}^k$ on $\boldsymbol{p}^k$.

4.2 LCM

If LCM is applied to the iteration scheme (39), we always let $\rho^{k+1} = \rho^{k+1}$=constant, and then solve for the incremental displacement degrees of freedom vector $\boldsymbol{p}$ caused by the incremental load vector $\rho\boldsymbol{q}$. But LCM the fits only to case where the set of finite elements has not reached the limit equlibrium state.

4.3 DCM

If DCM is appled to the iteration scheme (39), let ρ^{k+1} be unknown while the *i*th component p_i^{k+1} of $\boldsymbol{p}^{k+1}$ be known, namely,

$$p_i^{k+1} = \overline{p}_i \tag{42}$$

Considering the plastic deformation and the elastic deformation have the same tendency if the same load is applied to the system, we specify $\overline{p}_i$ as the maximum absolute component of vector $\boldsymbol{p}_q$, in which $\boldsymbol{p}_q$ is the elastic deformation due to the application of the incremental load vector $\boldsymbol{q}$ at the current load step, see Eq. (40).

By substituting Eq. (42) into the *i*th equation of Eq. (39) and solving for ρ^{k+1}, we have

$$\rho^{k+1} = \frac{\overline{p}_i - p_{ri}^k}{p_{qi}} \tag{43}$$

in which, p_{qi} and p_{ri}^k are the *i*th component of $\boldsymbol{p}_q$ and $\boldsymbol{p}_r^k$, see Eqs. (40) and (41), respectively.

Finally, the substitution of ρ^{k+1} calculated by Eq. (43) back to Eq. (39) will give rise to $\boldsymbol{p}^{k+1}$.

After each iteration, if

$$\left\|\boldsymbol{p}^{k+1} - \boldsymbol{p}^k\right\|_\infty < e_{\mathrm{p}}\left\|\boldsymbol{p}_q\right\|_\infty \tag{44}$$

is satisfied, the iteration process is terminated, and then the update of displacements and stresses is carried out, that is to say, $\boldsymbol{p}^{k+1}$ is added to the total node displacement vector and $\boldsymbol{\sigma}^{k+1}$ is assigned to $\boldsymbol{\sigma}_0$, and so on. e_{p} in Eq. (44) is the user specified relative tolerance.

As for the iterative initial value $\boldsymbol{p}^0$ of $\boldsymbol{p}$, it is feasible to take $\boldsymbol{p}_q$ caused by the incremental load vector $\boldsymbol{q}$ as $\boldsymbol{p}^0$, namely,

$$\boldsymbol{p}^0 = \boldsymbol{p}_q \tag{45}$$

Different from LCM which is applicable prior to the limit equilibrium state, DCM is applicable to the whole deformation history. The closer to the limit equilibrium state the discrete system is, the more efficient the DCM will be. If the discrete system is in the limit equilibrium state, the DCM has a surprising convergence rate: usually two or three iterations are needed to converge.

It can be seen from the above deduction that DCM and LCM have a highly analogous programming structure.

4.4 Algorithm FEPT for tracing the full equilibrium path

While evaluating the bearing capacity of a ground foundation or the factor of safety of a slope, it is necessary to bring the discrete system to the limit equilibrium state, i.e., to trace the full equilibrium path. The goal can be reached by consecutively invoking DCM. In the following, we call the algorithm FEPT, the acronym of "the Full Equilibrium Path Tracing".

Suppose ρ_i is the load multiplier after the *i*th invocation of DCM. Clearly, if ρ_i approaches zero, then the discrete system is nearly at the limit

equilibrium state. At this time,

$$\rho_L = \sum_i \rho_i \tag{46}$$

is the limit equilibrium multiplier relative to the incremental load $\boldsymbol{q}$.

The parameteric equation of path C with $(\boldsymbol{p}, \rho)$ acting as the coordinates in R^{n+1} is assumed to be

$$\boldsymbol{p} = \boldsymbol{p}(s), \quad \rho = \rho(s)$$

where s is the parameter taken by curve C. In general, we are incapable of having the analytical expression of curve C. By consecutively invoking DCM, however, what we will obtain a series of discrete points $(\boldsymbol{p}_k, \rho_k)$, $k = 1, 2, \cdots$, on curve C,

$$\boldsymbol{p}_k = \boldsymbol{p}(s_k), \rho_k = \rho(s_k) \tag{47}$$

If each invocation of DCM takes an equal elastic step $\overline{p}_i$, then parameters $s_k = k\overline{p}_i$, with $\overline{p}_i$ defined by Eq. (42) and the explanation just below it.

5 Application to slope stability analysis

In case of complicated failure modes, the deformation based finite element method is advantageous in many aspects over the classical limit analysis or the limit eqilibrium method. For example, if the critical slip surfaces of slopes cannot be simplified as lines, circular arcs or logarithmic spiral lines, the conventional limit analysis becomes very clumsy. Nevertheless, provided the slope is brought into the limit equilibrium state through strength reduction, the critical slip surface is able to be identified automatically. As such, the finite element strength reduction technique has been advocated by many researchers[18–28]. Some giant comercial software companies even have developed products based on this technique.

While a slope approaches the limit equilibrium state, the tenstion crack usually comes at the slope top. The slope stability factor will be reportedly overestimated by 70% if the tension crack is ignored in the stability analysis[23]. Duncan and Wright[24] proposed that a tension crack be set or a yield surface including tension-shear failure be used in case that tension stress is encountered.

In the traditional limit equilibrium method, the location and depth of the tension crack at the slope top are determined by a test-and-error technique, where numerous artificial assuptions are introduced[25].

In the limit analysis, the tension crack is regarded as part of the critical slip surface and the remaining is regarded as a logarithmic spiral line segment. The critical slip surface is obtained by minizing the critical height of the slope. Although the limit analysis fits only to simple failure modes, the upper bound method appears to become a little hot point since Michalowski [26], see refs. [27–29].

By applying a no tension cut-off Mohr-Coulomb criterion and the finite element strength reduction technique, in principle the tension cracks at the slope tops are able to be captured automatically. But the case is not like this. Till now, the finite element strength reduction technique has been limited within the intact Mohr-Coulomb criterion and the like, especially the Drucker-Prager yield surface. The reason for this is that non-smooth points are left after an intact yield surface is cut off its tension part, even if the yield surface itself is smooth, such as Drucker-Prager yield surface. Since essential difficulties have been overcome in the constitutive integration for plasticity with non-smooth yield surfaces, the tension cracks are expected to be captured using the finite element strength reduction technique.

Now we can realize one of advantages that the system of equilibrium equations is written in the form of Eq. (33) is to consider the influence of different stress paths on the slope stability.

Denoting by $\boldsymbol{\sigma}_0$ the initial stress field of the slope, the equivalent node load vector in balance with $\boldsymbol{\sigma}_0$ is

$$\boldsymbol{q}_0 = \sum_e \int_{\Omega^e} \boldsymbol{B}^{\mathrm{T}} \boldsymbol{\sigma}_0 \mathrm{d}\Omega \tag{48}$$

Suppose the incremental equivalent node load vector of the slope is $\boldsymbol{q}$, which might be caused by the quasi-static load due to the earthquake or by an excavation.

Using the algorithm FEPT in section 4.3, we can find the limit load multiplier ρ_{L} relative to $\boldsymbol{q}$. A different stabilization method will create different $\boldsymbol{q}$ and the relevant ρ_{L}. The larger ρ_{L} is, the safer the stabilization method will be.

5.1 Computation of safety of factor

Problems arising from both evaluating bearing capacity of ground foundations and analyzing stability of slopes belong to strength problems. But the evaluation of bearing capacity of a ground foundation is to bring the ground foundation into the limit equilibrium state through overloading while the strength and deformation parameters of soils are kept invariant. The bearing capacity of the ground foundation is measured by overloading factor ρ_{L}, which can be obtained by directly applying the algorithm FEPT. The analysis of slope stability is to bring the slope into the limit equilibrium state through strength reduction while the external loads are kept invariant. The slope stability is measure by the factor F of safety, which accordingly cannot be obtained by direct applying the algorithm FEPT.

Take the Mohr-Coulomb material as an instance. Suppose c and φ are the cohesion and inner frictional angle. The slope stability analysis is to find the strength reduction factor Z such that the slope will be at the limit equilibrium state if the strength parameters c and φ are replaced by c_Z and φ_Z, respectively, which are defined by

$$c_Z = \frac{c}{Z}, \quad \tan\varphi_Z = \frac{\tan\varphi}{Z} \tag{49}$$

While c and φ are reduced, it is proposed that Poisson's ratio ν be adjusted to ν_Z such that

$$\sin\varphi_Z \geqslant 1-2\nu_Z \tag{50}$$

The adjustment is very easy. Dassault has inserted the automatic adjustment process into its software product according to the adjustment procedure in ref.[30].

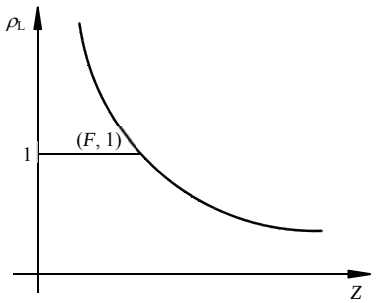

Fig. 4 Relationship between strength reduction factor Z and limit load multiplier ρ_L

For the given strength reduction factor Z, the limit load multiplier $\rho_L(Z)$ relative to load $\boldsymbol{q}$ can be found by invoking algorithm FEPT. Obviously $\rho_L(Z)$ is a strictly monotonically decreasing function, while the factor F of safety is just the unique root of the univariate equation $\rho_L(Z)=1$, as shown in Fig. 4. Using this fact, it is easy to design an algorithm for finding F by using the secant method; and also the factor of safety is unique if both the compatibility condition and the static admissibility condition are satisfied. The static admissibility condition demands that a stress field satisfies the equilibrium condition without violating the yield condition. The safety of safety has proved not to be not unique if the compatibility condition is not satisfied. For example, the factors of safety by the Morgenstern-Price method and the rigorous Bishop method are not always equal although the force systems caused by the two methods are both statically admissible.

5.2 Location of tension cracks at slope tops

Denote by ε_1 the major principal strain caused by the incremental load $\boldsymbol{q}$. Then, the tension region in a slope is the one in which $\varepsilon_1 \geqslant 0$. Part of the slope top is always tensioned. A tension crack should be at the position where ε_1 reaches the maximum. In this study, the following method is proposed to locate the tension crack. Find among all the elements the Gauss point G at which ε_1 reaches the maximum. Then, draw a vertical line passing point G. The part of the vertical line within the tension region at the slope top is specified as the vertical line.

6 Illustrative examples

The principle of the algorithm GSPC of constitutive integration for plasticity can be referred to [14], where more examples are given to illustrate the features of GSPC. So demonstrated here are applications of the proposed procedures to the stability analysis of slopes, particularly to the location of tension cracks at the top of slopes. More sophisticated slope examples are available in [9].

6.1 A homogeneous soil slope

Figure 5(a) shows a homogeneous soil slope with a height of 20 m and a slope angle of 45°, designed by Cheng et al in [31]. The soil has a unit weight γ = 25 kN/m^3, cohesion c = 42 kPa, internal friction angle φ = 30°, Young's modulus E = 30 MPa, Poisson's ratio ν = 0.3. Figure 5(b) displays the finite element mesh with the left and right boundaries smoothly supported and the bottom fixed both horizontally and vertically. All the elements in the mesh are quadrilateral elements. Integration over each element is 2×2 order Gaussian quadrature. The tolerance in DCM is e_p = 1%, see Eq. (44).

Let F^s_{MC} and F^s_{Cut} represent the factors of safety by using the intact the Mohr-Coulomb yield surface and the tension cut-off Mohr-Coulomb yield surface, respectively.

The outcomes of F^s_{MC} = 1.537 and F^s_{Cut} = 1.512 imply that ignoring tension failure overestimates the factor of safety only by 1.65%, an error completely acceptable for engineering.

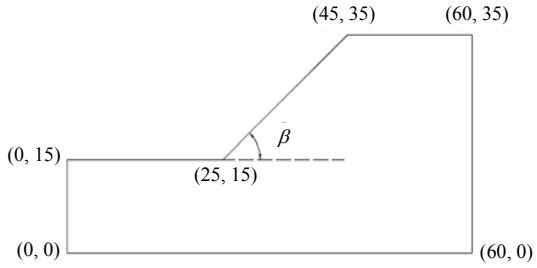

(a) Model geometry（unit: m）

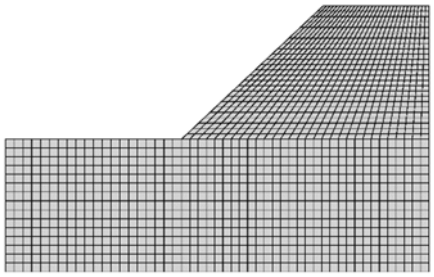

(b) A mesh configuration

Fig. 5 Model geometry and mesh configuration

Figure 6 displays the distribution of the equivalent plastic strain $\bar{\varepsilon}_p$ at the moment when the slope reaches the limit equilibrium state, defined by,

$$\bar{\varepsilon}_p = \sum\sqrt{\frac{2}{3}\Delta\boldsymbol{\varepsilon}_p^T\Delta\boldsymbol{\varepsilon}_p} \tag{51}$$

where the summation is with respect to all the incremental steps, and $\Delta\boldsymbol{\varepsilon}_p$ the incremental plastic strain vector within a typical step.

Figure 6 also displays the tension zone Ω_T at the top of the slope in the limit equilibrium state.

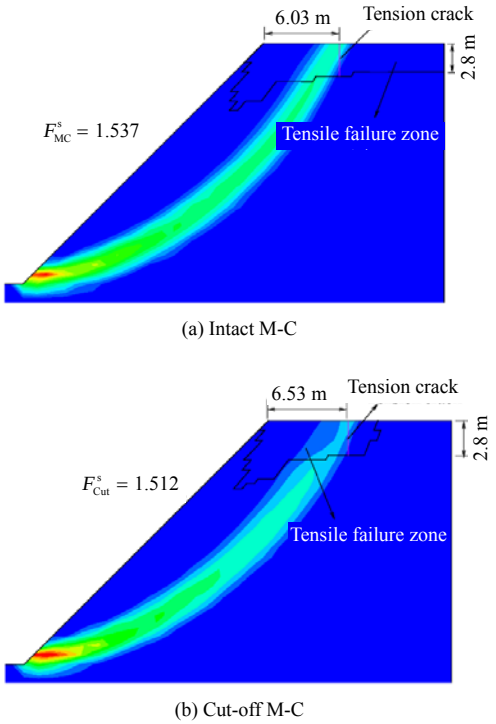

Fig. 6 Comparison of failure mechanism (1 500 elements)

Figure 6(a) clearly tells us that ignoring the tensile failure brings about the tension zone Ω_T at the slope top extending to the left boundary. Further increasing model dimensions does not work and still Ω_T extends to the right boundary of the model. This is an abnormal phenomenon familiar to those who have some experiences of using the finite element strength reduction, which is usually believed the effect of finite model dimensions. Considering the tension failure causes a smaller Ω_T in Fig. 6(b), seemingly more reasonable. Further, included in Fig. 6 are the tension cracks, which are determined by the method in section 5.2.

The influence of mesh density is shown in Fig. 7, suggesting that with increasing mesh density,

1) the failure zone becomes narrower and narrower;

2) the factor of safety becomes smaller and smaller. This is because the FEM we are using is based on compatible displacement elements and always approaches from below the exact displacement. Under the same external load level, certainly a larger deformation field results in a more dangerous slope and, as a result, the factor of safety is smaller.

and 3) the location and depth of the tension crack converges prior to the failure zone; for example, at least at the mesh density of 1500 elements, the location and depth of the tension crack have become convergent, yet the failure zone have not.

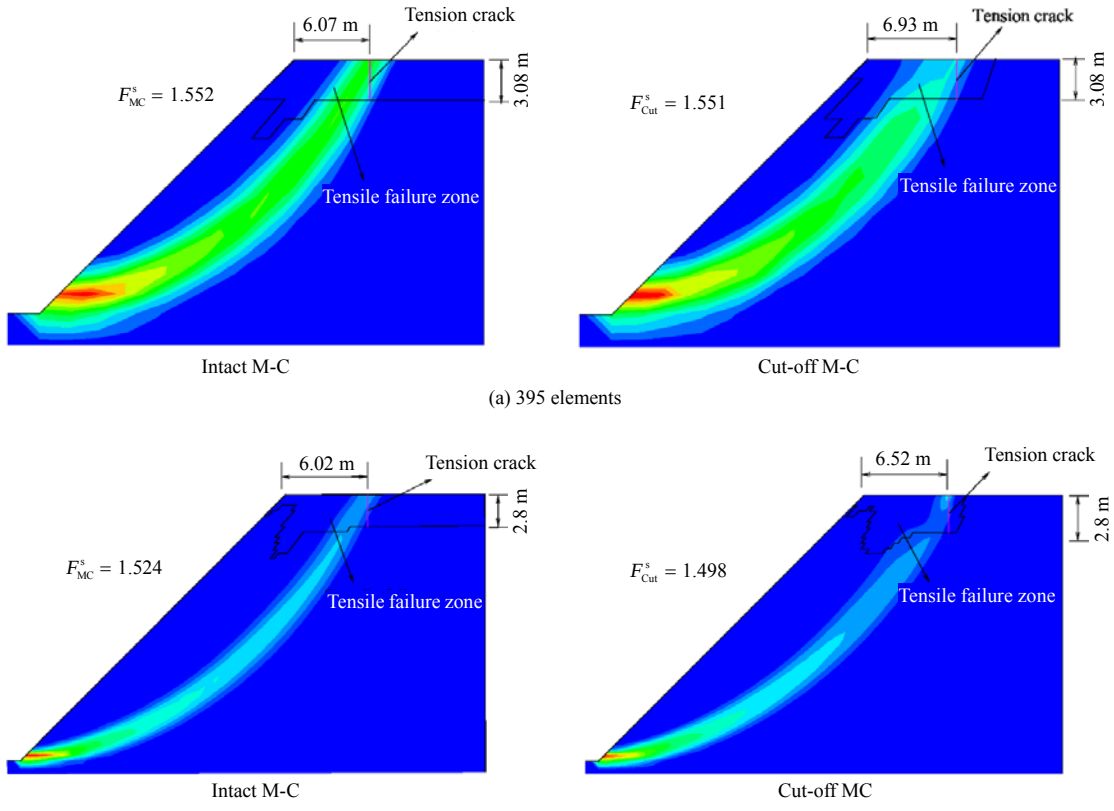

Fig. 7 Influence of mesh density

The depth of tension cracks of slopes in the limit equilibrium state is still an open issue in theory. There have been many works on this issue. For example, Michalowski proposed in [26] an empirical interval of the depth of tension cracks for homogeneous slopes with no water

$$h=\frac{\kappa c_{\mathrm{m}}}{\gamma}\tan\left(\frac{\pi}{4}+\frac{\varphi_{\mathrm{m}}}{2}\right) \tag{52}$$

where κ varies between 2 and 3.83; c_{m} and φ_{m} are the mobilized strength parameters, namely,

$$c_{\mathrm{m}}=\frac{c}{F_{\mathrm{s}}},\quad \tan\varphi_{\mathrm{m}}=\frac{\tan\varphi}{F_{\mathrm{s}}} \tag{53}$$

By taking $F_{\mathrm{s}}=F_{\mathrm{Cut}}^{\mathrm{s}}=1.512$, the h-interval evaluated by Eq. (52) is (3.23 m, 6.18 m). To the authors' view the interval is too large.

The convergent depth estimated by the proposed analysis is 2.80 m, even below the lower bound of 3.23 m evaluated by Eq. (52). In the following, we will show Eq. (52) exaggerates the depth of tension cracks.

6.2 Influence of slope angle

With the same mechanical parameters as the above example, let the slope angle β be 50°, 60°, 70°, 80° and 90°. Table 1 lists the results, suggesting that before β exceeds 70° the difference in the factor of safety can be ignored using the intact M-C surface or the cut-off M-C surface. If β >80°, the difference increases sharply, and reaches 20% at β =90°. Consequently, the stability of deep foundation pits must be analyzed under the condition of tensile strength cut-off.

Table 1 Outcomes of different slope angles

Angle /(°)	$F_{\mathrm{MC}}^{\mathrm{s}}$	$F_{\mathrm{Cut}}^{\mathrm{s}}$	Difference /%
45	1.512	1.537	1.63
50	1.386	1.412	1.84
60	1.180	1.218	3.12
70	1.012	1.060	4.53
80	0.851	0.928	8.30
90	0.652	0.814	19.9

By taking $F_{\mathrm{s}}=F_{\mathrm{Cut}}^{\mathrm{s}}=1.06$ corresponding to β = 70°, the interval of the tension crack depth is (17.02 m, 32.60 m) according to the evaluation (52), while the slope height is only 20 m, and thus Michalowski's overestimation is concluded. The depth evaluated by the proposed procedure is 4.8 m, a seemingly more practical value, displayed in Fig. 8.

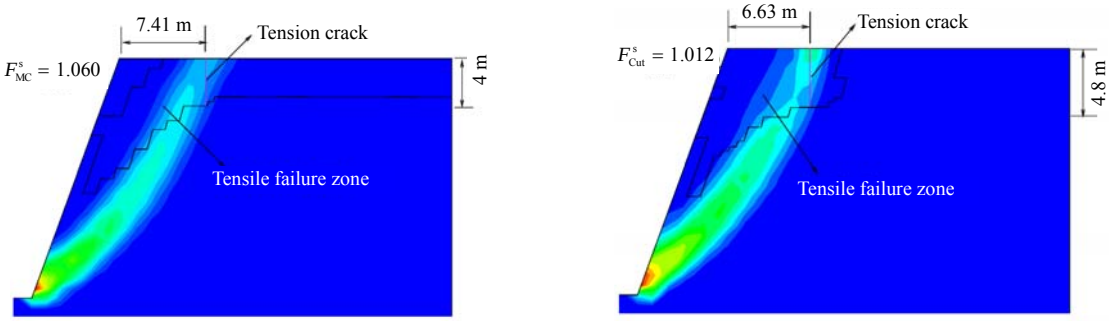

(a) Intact M-C (b) Cut-off M-C

Fig. 8 Failure mechanism comparison (β=70°)

7 Conclusions

On the basis of assumption of elastic perfectly plastic deformation, we conclude:

1) The relationship between stresses and strains in the rate form can be reduced to a system of differential complementary equations, DCE for short.

2) For the associated flow rule, the solution to the DCE is existent and unique; for the non-associated flow rule with the no tension cut-off Mohr-Coulomb surface, the solution to the DCE is existent and unique, either.

3) When one of the conditions in item 2) is satisfied, the Gauss-Seidel iteration based projection-contraction algorithm, GSPC, is always convergent for arbitrary large strain increments, but irrelevant to whether the yield surface is smooth or not. Furthermore, the algorithm GSPC is advantageous in robustness and solution efficiency over the return-mapping algorithm.

4) The solver, which is designed for the system of equilibrium equations by utilizing the decomposition of elastic-plastic stresses, i.e., Eq. (16), enables the load controlled method (LCM) to have the similar programming structure to the displacement controlled method (DCM), in which DCM is able to bring stably and efficiently the discrete system into the limit equilibrium state.

5) The factor of safety is unique as long as the relevant stress field is deformation compatibility condition and static admissibility condition.

In addition, the formula for computing partial derivatives of principal stresses with respect to component stresses simplifies the constitutive integration, and seemingly fills a gap in the stress analysis.

It is worth noting the theory and algorithm for constitutive integration of plasticity apply only to the case of elastic–perfectly plastic materials. Now we are investigating the constitutive integration of plasticity with hardening or softening flow rule, and will have relevant results to come.

References

[1] CLAUSEN J, DAMKILDE L, ANDERSEN L. Efficient return algorithms for associated plasticity with multiple yield planes[J]. International Jounal for Numerical Methods Engineering, 2006, 66(6): 1036–1059.

[2] SLOAN S W, ABBO A J, SHENG D. Refined explicit

integration of elastoplastic models with automatic error control[J]. Engineering Computations, 2001, 18(1-2): 121–194.

[3] ZHENG Ying-ren, KONG Liang, ABI Erdi. Strength theory and numerical limit analysis[M]. Beijing: Science Press, 2020.

[4] ZIENKIEWICZ O C, PANDE G N. Some useful forms of isotropic yield surface for soil and rock mechanics[M]// Finite Elements in Geomechanics, Chapter 5. London: Wiley, 1977: 179–198.

[5] MENETREY P, WILLAM K. Triaxial failure criterion for concrete and its generalization[J]. ACI Structural Journal, 1995, 92(3): 311–318.

[6] ABBO A J, LYAMIN A V, SLOAN S W, et al. A C2 continuous approximation to the Mohr-Coulomb yield surface[J]. International Journal of Solids and Structures, 2011, 48: 3001–3010.

[7] WILKINS A, SPENCER B W, JAIN A, et al. A method for smoothing multiple yield functions[J]. Interntional Journal for Numerical Methods in Engineering, 2020, 121: 434–449.

[8] OWEN D R J, HINTON E. Finite elements in plasticity: theory and practice[J]. Applied Ocean Research, 1981, 3(3): 149.

[9] ZHANG Tan. Constitutive integration of plasticity with non-smooth yield surfaces and applications to strength problems[D]. Beijing: Beijing University of Technology, 2020.

[10] DE SOUZA NETO E A, PERIĆ D, OWEN D R J. Computational methods for plasticity: theory and applications[M]. Chichester: Wiley, 2008.

[11] SIMO J C, HUGHES T J R. Computational inelasticity[M]. New York: Springer, 1998.

[12] ZIENKIEWICZ O C, TAYLOR R L. The finite element method: solid mechanics[M]. 2nd ed. London, UK: McGraw-Hill Book Company, 1991.

[13] ASCHER U M, PETZOLD L R. Computer methods for ordinary differential equations and differential-algebraic equations[M]. Philadelphia: SIAM, 1998.

[14] ZHENG H, ZHANG T, WANG Q S. The mixed complementarity problem arising from non-associative plasticity with non-smooth yield surfaces[J]. Computer Methods in Applied Mechanics and Engineering, 2020, 361: 112756.

[15] HE B S. A class of projection and contraction methods for monotone variational inequalities[J]. Applied Mathematics and Optimization,1997, 35: 69–76.

[16] YANG Guang-hua, LI Guang-xin, JIE Yu-xin. Generalized potential theorey fo constitution models of soils with applications[M]. Beijing: China Water & Power Press, 2017.

[17] ZHENG H, LIU D F, LI C G. On the assessment of failure in slope stability analysis by the finite element method[J]. Rock Mechanics and Rock Engineering, 2008, 41: 629–639.

[18] MATSUI T, SAN K C. Finite element slope stability analysis by shear strength reduction technique[J]. Soils and Foundations, 1992, 32: 59–70.

[19] UGAI K, LESHCHINSKY D. Three-dimensional limit equilibrium and finite element analyses: a comparison of results[J]. Soils and Foundations, 1995, 35: 1–7.

[20] GRIFFITHS D V, LANE P A. Slope stability analysis by finite elements[J]. Geotechnique, 1999, 49: 387–403.

[21] DAWSON E M, ROTH W H, DRESCHER A. Slope stability analysis by strength reduction[J]. Geotechnique, 1999, 49: 835–840.

[22] YANG Y T, SUN G H, ZHENG H. Stability analysis of soil-rock-mixture slopes using the numerical manifold method[J]. Engineering Analysis with Boundary Elements, 2019, 109: 153–160.

[23] MICHALOWSKI R L. Stability of intact slopes with tensile strength cut-off[J]. Geotechnique, 2017, 67(8): 720–727.

[24] DUNCAN J M, WRIGHT G S, BRANDON L T. Soil strength and slope stability[M]. 2nd ed. Hoboken: Wiley, 2014.

[25] SPENCER E. Effect of tension on the stability of embankments[J]. Journal of the Soil Mechanics and Foundation Division, 1968, 94: 1159–1173.

[26] MICHALOWSKI R L. Stability assessment of slopes with cracks using limit analysis[J]. Canadian Geotechnical Journal, 2013, 50(10): 1011–1021.

[27] UTILI S. Investigation by limit analysis on the stability of slopes with cracks[J]. Geotechnique, 2013, 63(2): 140–154.

[28] PARK D, MICHALOWSKI R L. Three-dimensional stability analysis of slopes in hard soil/soft rock with tensile strength cut-off[J]. Engineering Geology, 2017, 229: 73–84.

[29] MICHALOWSKI R L. Failure potential of infinite slopes in bonded soils with tensile strength cut-off[J]. Canadian

Geotechnical Journal, 2018, 55(4): 477–485.

[30] ZHENG Hong, LI Chun-guang, LEE C F, et al. Finite element method for solving the factor of safety[J]. Chinese Journal of Geotechnical Engineering, 2002, 24(5): 626–629.

[31] CHENG Y M, LANSIVAARA T, WEI W B. Two-dimensional slope stability analysis by limit equilibrium and strength reduction methods[J]. Computers and Geotechnics, 2007, 34(3): 137–150.

Appendix Algorithm of GSPC

The algorithm GSPC for MiCP$\left(\boldsymbol{f}_I, \boldsymbol{f}_E\right)$ defined in Eq. (17) is invoked in this way:

$$\left(\boldsymbol{\lambda}, \boldsymbol{\sigma}\right) = \mathrm{GSPC}\left(\boldsymbol{\lambda}^0, \boldsymbol{\sigma}^0\right) \quad (A1)$$

The input arguments of $\boldsymbol{\lambda}^0$ and $\boldsymbol{\sigma}^0$ are the initial guess of $\boldsymbol{\lambda}$ and $\boldsymbol{\sigma}$, respectively. In general, $\boldsymbol{\lambda}^0$=0, $\boldsymbol{\sigma}^0 = \boldsymbol{\sigma}_e$, with $\boldsymbol{\sigma}_e$ defined in Eq.(14). Here and subsequently, all the notations are explained in the text.

The pseudocodes of GSPC are listed as follows, in which //2* represents this is the second note to be explained after the codes, and so on.

Step 0: Let $\beta_I = \beta_E = 1$; $k = 0$;

Step 1: $\bar{\boldsymbol{\lambda}} = \max\left[\boldsymbol{\lambda} - \beta_I \boldsymbol{f}_I\left(\boldsymbol{\lambda}, \boldsymbol{\sigma}\right), 0\right]$; //1*

$$\bar{\boldsymbol{\sigma}} = \boldsymbol{\sigma} - \beta_E \boldsymbol{f}_E\left(\bar{\boldsymbol{\lambda}}, \boldsymbol{\sigma}\right);$$

if $\left\|\bar{\boldsymbol{\lambda}} - \boldsymbol{\lambda}\right\|_\infty \leqslant \varepsilon_\lambda \left\|\bar{\boldsymbol{\lambda}}\right\|_\infty$ and $\left\|\bar{\boldsymbol{\sigma}} - \boldsymbol{\sigma}\right\|_\infty \leqslant \varepsilon_\sigma \left\|\bar{\boldsymbol{\sigma}}\right\|_\infty$ //2*

then $\boldsymbol{\lambda} = \bar{\boldsymbol{\lambda}}$; $\boldsymbol{\sigma} = \bar{\boldsymbol{\sigma}}$; break;

$$r_\lambda = \frac{\beta_I \left\|\boldsymbol{f}_I\left(\boldsymbol{\lambda}, \boldsymbol{\sigma}\right) - \boldsymbol{f}_I\left(\bar{\boldsymbol{\lambda}}, \boldsymbol{\sigma}\right)\right\|_2}{\left\|\boldsymbol{\lambda} - \bar{\boldsymbol{\lambda}}\right\|_2}; \quad //3*$$

while $r_\lambda > \nu$ //4*

$$\beta_I = \frac{2}{3}\beta_I \min\left(1, \frac{1}{r_\lambda}\right); \quad \bar{\boldsymbol{\lambda}} = \max\left[\boldsymbol{\lambda} - \beta_I \boldsymbol{f}_I\left(\boldsymbol{\lambda}, \boldsymbol{\sigma}\right), 0\right];$$

$$r_\lambda = \frac{\beta_I \left\|\boldsymbol{f}_I\left(\boldsymbol{\lambda}, \boldsymbol{\sigma}\right) - \boldsymbol{f}_I\left(\bar{\boldsymbol{\lambda}}, \boldsymbol{\sigma}\right)\right\|_2}{\left\|\boldsymbol{\lambda} - \bar{\boldsymbol{\lambda}}\right\|_2};$$

end(while);

$$r_\sigma = \frac{\beta_E \left\|\boldsymbol{f}_E\left(\bar{\boldsymbol{\lambda}}, \boldsymbol{\sigma}\right) - \boldsymbol{f}_E\left(\bar{\boldsymbol{\lambda}}, \bar{\boldsymbol{\sigma}}\right)\right\|_2}{\left\|\boldsymbol{\sigma} - \bar{\boldsymbol{\sigma}}\right\|_2};$$

while $r_\sigma > \nu$

$$\beta_E = \frac{2}{3}\beta_E \min\left(1, \frac{1}{r_\sigma}\right); \quad \bar{\boldsymbol{\sigma}} = \boldsymbol{\sigma} - \beta_E \boldsymbol{f}_E\left(\bar{\boldsymbol{\lambda}}, \boldsymbol{\sigma}\right);$$

$$r_\sigma = \frac{\beta_E \left\|\boldsymbol{f}_E\left(\bar{\boldsymbol{\lambda}}, \boldsymbol{\sigma}\right) - \boldsymbol{f}_E\left(\bar{\boldsymbol{\lambda}}, \bar{\boldsymbol{\sigma}}\right)\right\|_2}{\left\|\boldsymbol{\sigma} - \bar{\boldsymbol{\sigma}}\right\|_2};$$

end(while);

$$\boldsymbol{d}_\lambda\left(\boldsymbol{\lambda}, \bar{\boldsymbol{\lambda}}\right) = \left(\boldsymbol{\lambda} - \bar{\boldsymbol{\lambda}}\right) - \beta_I\left[\boldsymbol{f}_I\left(\boldsymbol{\lambda}, \boldsymbol{\sigma}\right) - \boldsymbol{f}_I\left(\bar{\boldsymbol{\lambda}}, \boldsymbol{\sigma}\right)\right];$$

$$\alpha = \frac{\left(\boldsymbol{\lambda} - \bar{\boldsymbol{\lambda}}\right)^{\mathrm{T}} \boldsymbol{d}_\lambda\left(\boldsymbol{\lambda}, \bar{\boldsymbol{\lambda}}\right)}{\left\|\boldsymbol{d}_\lambda\left(\boldsymbol{\lambda}, \bar{\boldsymbol{\lambda}}\right)\right\|_2^2}; \quad \boldsymbol{\lambda} = \boldsymbol{\lambda} - \gamma\alpha \boldsymbol{d}_\lambda\left(\boldsymbol{\lambda}, \bar{\boldsymbol{\lambda}}\right); \quad //5*$$

if $r_\lambda \leqslant \mu$ then $\beta_I = 1.5\beta_I$; //6*

$$\boldsymbol{d}_\sigma\left(\boldsymbol{\sigma}, \bar{\boldsymbol{\sigma}}\right) = \left(\boldsymbol{\sigma} - \bar{\boldsymbol{\sigma}}\right) - \beta_{\mathrm{E}}\left[\boldsymbol{f}_{\mathrm{E}}\left(\bar{\boldsymbol{\lambda}}, \boldsymbol{\sigma}\right) - \boldsymbol{f}_{\mathrm{E}}\left(\bar{\boldsymbol{\lambda}}, \bar{\boldsymbol{\sigma}}\right)\right];$$

$$\alpha = \frac{\left(\boldsymbol{\sigma} - \bar{\boldsymbol{\sigma}}\right)^{\mathrm{T}} \boldsymbol{d}_\sigma\left(\boldsymbol{\sigma}, \bar{\boldsymbol{\sigma}}\right)}{\left\|\boldsymbol{d}_\sigma\left(\boldsymbol{\sigma}, \bar{\boldsymbol{\sigma}}\right)\right\|_2^2}; \quad \boldsymbol{\sigma} = \boldsymbol{\sigma} - \gamma\alpha \boldsymbol{d}_\sigma\left(\boldsymbol{\sigma}, \bar{\boldsymbol{\sigma}}\right);$$

if $r_\sigma \leqslant \mu$ then $\beta_{\mathrm{E}} = 1.5\beta_{\mathrm{E}}$;

Step 2. $k = k + 1$; go to Step 1.

//1*

Suppose $\boldsymbol{a} = \left(a_i\right)$ and $\boldsymbol{b} = \left(b_i\right)$ are two given vectors of the same dimension, the expression

$$\boldsymbol{c} = \max\left(\boldsymbol{a}, \boldsymbol{b}\right) \quad (A2)$$

generates the vector $\boldsymbol{c} = \left(c_i\right)$ of the same dimension as vector $\boldsymbol{a}$, with $c_i = \max\left(a_i, b_i\right)$.

//2*

1) Suppose $\boldsymbol{x}$ is *n*-dimensional vector with components of $x_1, \cdots, x_n$, then

$$\left\|\boldsymbol{x}\right\|_\infty = \max\left(x_1, \cdots, x_n\right).$$

2) ε_λ and ε_σ are the relative error tolerances of $\boldsymbol{\lambda}$ and $\boldsymbol{\sigma}$, with $\varepsilon_\lambda = \varepsilon_\sigma = 10^{-4}$ say, a very high precision control.

//3*

Suppose $\boldsymbol{x}$ is *n*-dimensional vector with components of $x_1, \cdots, x_n$, then

$$\left\|\boldsymbol{x}\right\|_2 = \left(x_1^2, \cdots, x_1^2\right)^{\frac{1}{2}} \quad (A3)$$

//4*, //5* and //6*

According to He [15], parameter $\nu = 0.9$, parameter $\gamma = 1.9$, parameter $\mu = 0.4$.